Received: 17 March 2017 | Revised: 13 July 2017 | Accepted: 8 September 2017

DOI: 10.1002/stc.2107

RESEARCH ARTICLE

WILEY

Structural damage detection based on l_1 regularization using natural frequencies and mode shapes

Rongrong Hou[1] | Yong Xia[1] | Xiaoqing Zhou[2]

[1] Department of Civil and Environmental Engineering, The Hong Kong Polytechnic University, Kowloon, Hong Kong

[2] College of Civil Engineering, Shenzhen University, Shenzhen, China

Correspondence
Yong Xia, Department of Civil and Environmental Engineering, The Hong Kong Polytechnic University, Kowloon, Hong Kong
Email: ceyxia@polyu.edu.hk

Funding information
Hong Kong Polytechnic University, Grant/Award Number: 1-ZVDN and G-YBHL; National Natural Science Foundation of China, Grant/Award Number: 51678364; PolyU Research Grant

Summary

Conventional vibration-based damage detection methods employ the Tikhonov regularization in model updating to deal with the problems of underdeterminacy and measurement noise. However, the Tikhonov regularization technique tends to provide over smooth solutions that the identified damage is distributed to many structural elements. This result does not match the sparsity property of the actual damage scenario, in which structural damage typically occurs at a small number of locations only in comparison with the total elements of the entire structure. In this study, an l_1 regularization-based model updating technique is developed by utilizing the sparsity of the structural damage. Both natural frequencies and mode shapes are employed during the model updating. A strategy of selecting the regularization parameter for the l_1 regularization problem is also developed. A numerical and an experimental examples are utilized to demonstrate the effectiveness of the proposed damage detection method. The results showed that the proposed l_1 regularization-based method is able to locate and quantify the sparse damage correctly over a large number of elements. The effects of the mode number on the damage detection results are also investigated. The advantage of the present l_1 regularization over the traditional l_2 regularization method in damage detection is also demonstrated.

KEYWORDS

damage detection, l_1 regularization, model updating, sparsity, vibration methods

1 | INTRODUCTION

Numerous vibration-based structural damage detection methods have been developed over the past decades.[1,2] The basic idea of these methods is that structural damage may induce changes in vibration characteristics, such as frequencies,[3,4] mode shapes,[5,6] and their variants.[7–9]

Civil structures are generally large in size and contain a large number of components. However, the number of available vibration measurements is limited. To avoid this underdetermined problem in mathematics, superelements are usually employed in both numerical modeling and model updating. The use of such elements hinders the local small damage from being directly quantified with the updating parameter of the entire superelement. In addition, the sensitivity-based model updating for damage detection is usually ill-posed. A small perturbation in the input data (for example, measurement noise) would lead to a significant change in the solution. Therefore, most vibration-based damage detection methods employ the Tikhonov regularization (or l_2 regularization) to deal with this problem.[10–12] The Tikhonov

regularization tends to produce over smooth solutions and causes the identified damage distributed to many structural elements. However, this is not consistent with the practical situation that damage usually occurs in a few sections or members only especially at the early stage. For example, structural early damage tends to appear in some column ends or the midspan of beams where the maximum stresses are located. For steel structures, fatigue damage usually occurs at a few fatigue-critical members only.

The small number of damage locations can be treated as sparsity as compared with the total elements of the entire structure. Therefore, the identification of the damaged elements is a sparse recovery problem. According to the sparse recovery theory, the sparse vector of which only a few entries are nonzero can be recovered using a small number of measurement data only. However, this sparse recovery theory has seldom been utilized in previous damage detection until recently due to the booming of compressive sensing (CS).[13–15] Bao *et al*. first introduced the CS technology to structural health monitoring (SHM) and conducted a series of applications of CS to SHM, including data compression,[16] recovery of lost data for wireless sensors,[17,18] identification of moving load distribution,[19] and wireless sensor development.[20] Wang and Hao[21] discussed some potential applications of CS in structural engineering. Yang and Nagarajaiah have applied the CS technique for denoising structural vibration responses[22] and modal identification.[23,24] Huang *et al*.[25] investigated the robustness property of the Bayesian CS technique in SHM.

More recently, several researchers have applied the sparse recovery theory to structural damage detection. Bao *et al*.[26] proposed the application of CS technology for structure damage detection. Yang and Nagarajaiah[27] developed a damage identification method based on sparse representation and CS, in which modal features were expressed as a sparse linear combination of the bases of an over-complete reference feature dictionary. Hernandez[28] expanded the sensitivity-based model updating using l_1 norm minimization to localize and quantify isolated structural damage. The change in a subset of eigenvalues of the system was selected as the damage sensitive feature. Zhou *et al*.[29] applied the l_1 regularization approach to detect structural damage using the first few frequency data. Parametric studies were conducted to investigate the effects of measurement number, damage severity, number of damage, and noise level on the damage detection results. Zhang and Xu[30] compared the damage identification results using Tikhonov regularization and sparse regularization in time-domain.

The above vibration-based damage detection methods utilizing the sparsity of structural damage either use natural frequency only or time-history acceleration responses or numerical data. Using the time-domain data for damage identification is not efficient as the calculation of the structural responses is time-consuming. Frequencies are usually not sensitive to local damage, and the small frequency changes caused by structural damage tend to be masked by the noise in the measurement data. In general, mode shapes could provide spatial information and are thus more sensitive to local damage. This study extends the authors' former work based on the frequency changes[29] and develops the l_1 regularization technique for structural damage identification using both frequencies and mode shapes. A selection criterion of the regularization parameter for the l_1 regularization problem is developed. The effectiveness of the proposed method is demonstrated through applications to a numerical planar truss and an experimental frame.

2 | DAMAGE DETECTION USING L_1-REGULARIZED MODEL UPDATING

2.1 | Sensitivity-based model updating

Sensitivity-based model updating is to find changes in structural parameters through minimizing the discrepancy between analytical predictions and experimental data.[31,32] Under the assumption that the structure behaves linearly before and after damage, the relationship between damage parameters $\{p\}$ and changes of modal parameters $\{\Delta R\}$ can be expressed as[31,33]

$$[S]\{p\} = \{\Delta R\} = \{R^E\} - \{R^0\} \tag{1}$$

where $\{R^E\}$ and $\{R^0\}$ refer to the measured modal parameters and the analytical ones, respectively, and [S] is the sensitivity matrix defined as the derivative of the modal parameters with respect to the damage parameters. The sensitivity matrix of the eigenvalue and mode shape can be expressed as

$$[S_\lambda] = \frac{\partial\{\lambda\}}{\partial\{p\}} \tag{2}$$

$$[S_\phi] = \frac{\partial\{\phi\}}{\partial\{p\}} \tag{3}$$

where $\{\lambda\}$ and $\{\phi\}$ are eigenvalues and eigenvectors, respectively. [S] can be calculated either from the global finite element (FE) model[34] or using the substructuring approach.[35,36]

The damage parameters $\{p\}$ can be calculated by solving the below optimization problem

$$\min_{\{p\}\in R^N} \|[S]\{p\}-\{\Delta R\}\|_2^2 \tag{4}$$

Equation 4 can be rewritten as

$$\min_{\{p\}\in R^N} \|\{R(p)\}-\{R^E\}\|_2^2 \tag{5}$$

where $\{R(p)\}$ is the analytical modal parameters. The above inverse problem is typically ill-conditioned and a small perturbation in the input data (e.g., measurement noise) would lead to significant changes in the solution. To deal with this problem, the Tikhonov regularization is commonly used in the model updating. That is, a regularization term is added in the objective function as

$$\min_{\{p\}\in R^N} \|\{R(p)\}-\{R^E\}\|_2^2 + \beta \|\{p\}\|_2^2 \tag{6}$$

where $\|\{R(p)\}-\{R^E\}\|_2^2$ is the data-fitting term or residual norm indicating how the updated parameters fit the data, $\|\{p\}\|_2^2$ is the regularization term or solution norm quantifying the solution, and $\beta > 0$ is the regularization parameter. In general, the regularization parameter β is not known a priori and has to be determined based on the problem. Because the Tikhonov regularization has the closed-form solution, there are tractable methods for choosing the regularization parameters such as the well-known L-curve criterion.[37] The criterion utilizes a parametric plot of the solution norm versus the residual norm for different β, which looks like an "L" shape in the log–log scale. The corner of the L-shaped curve is regarded as the balance between the solution norm and the residual norm, and thus, the corresponding β value is determined as the optimal regularization parameter. Equation 6 is commonly referred to as Tikhonov regularization or l_2 regularization as the 2-norm is used.

2.2 | Sparse damage detection using frequencies and mode shapes

The structural stiffness matrix in the undamaged state can be expressed in the following form

$$[K] = \sum_{i=1}^{n} \alpha_i [K^i] \tag{7}$$

where $[K^i]$ is the ith element stiffness matrix and α_i is the element stiffness parameter. The existing damage detection methods usually assume that there will be a detectable change in stiffness with the mass remaining unchanged, and the change in damping may be disregarded.[38] Therefore, only the element stiffness parameter reduces when damage occurs under this assumption. The structural stiffness matrix in the damaged state takes the following form

$$\left[\widetilde{K}\right] = \sum_{i=1}^{n} \widetilde{\alpha}_i [K^i] \tag{8}$$

where $\widetilde{\alpha}_i$ is the element stiffness parameter in the damaged state.

The stiffness reduction factor (SRF) is then defined as[6,29]

$$p_i = \frac{\widetilde{\alpha}_i - \alpha_i}{\alpha_i} \tag{9}$$

The SRF is chosen as the damage parameter in this study, and the values of SRF indicate both damage location and damage severity. $\{p\}$ is a sparse vector with several non-zero items at the damaged locations but with many zeros at others. $p_i = 0$ indicates that the ith element is intact; whereas $p_i = -1$ means the element is completely damaged.

Taking into account the sparsity of the structural damage, the following l_1 regularization instead of the Tikhonov regularization is introduced to not only stabilize the ill-posed problem in Equation 5 but also enforce sparsity in the solution

$$\min_{\{p\}\in R^N} \left\|\{R(p)\}-\left\{R^E\right\}\right\|_2^2 + \beta\|\{p\}\|_1 \tag{10}$$

where $\|\cdot\|_1$ is the 1-norm and thus $\|\{p\}\|_1$ is referred to as the l_1 regularization term. Although the objective function in Equation 10 is convex, it is not differentiable and thus more computational effort is required.[39]

This study utilizes both natural frequencies and mode shapes in model updating for damage detection. Based on Equation 10, the optimization problem is rewritten as

$$\widehat{p} = \arg\min_{\widehat{p}}\left(\frac{1}{m}\sum_{i=1}^{m}\left[\frac{{\lambda_i}^A(\{p\})-{\lambda_i}^E}{{\lambda_i}^E}\right]^2 + \frac{1}{m\times np}\sum_{i=1}^{m}\sum_{j=1}^{np}\left[{\phi_{ji}}^A(\{p\})-{\phi_{ji}}^E\right]^2 + \frac{\beta}{n}\|\{p\}\|_1\right) \tag{11}$$

where $\{\lambda_i\}$ and $\{\phi_{ji}\}$ are the ith eigenvalues and corresponding mode shape at jth point, respectively, m is the number of measured modes, np is the number of measurement points, n is the number of elements in the FE model, and subscripts "A" and "E" represent the items from the analytical model and experiment, respectively. Here, the eigenvalue residual, eigenvector residual, and the regularization term are divided by the length of the vectors (i.e., m, $m \times np$, and n, respectively) to make these three parts comparable.

Because mode shapes are dimensionless and may differ by a constant, direct comparison of two mode shape vectors with different scales may cause the results completely incorrect. In this connection, the mode shapes calculated from the FE model should be adjusted such that they are in the same direction and same scale as the measured mode shapes, through the modal scale factor as defined as follows[40]

$$MSF\left(\left\{\widetilde{\phi}_i^{\,A}\right\},\left\{\phi_i^{\,E}\right\}\right) = \frac{\left\{\widetilde{\phi}_i^{\,A}\right\}^T\left\{\phi_i^{\,E}\right\}}{\left\{\widetilde{\phi}_i^{\,A}\right\}^T\left\{\widetilde{\phi}_i^{\,A}\right\}} \tag{12}$$

$$\left\{\phi_i^{\,A}\right\} = \left\{\widetilde{\phi}_i^{\,A}\right\}\times MSF \tag{13}$$

where $\left\{\widetilde{\phi}_i^{\,A}\right\}$ is the ith calculated mode shape before adjustment.

2.3 | Selection of regularization parameter

One critical issue in solving the optimization problem of Equation 11 is the selection of the regularization parameter β. For a large regularization parameter, the second term $\beta\|\{p\}\|_1$ will dominate the objective function and thus be penalized more severely during the optimization process compared to the data-fitting term $\left\|R(\{p\})-\left\{R^E\right\}\right\|_2^2$. As a result, the solution ($\|\{p\}\|_1$) tends to decrease. When β exceeds a threshold $\beta_{\max}$, the solution becomes zero.[41] Therefore, with the increase of the regularization parameter β, the solution norm will decrease and the residual norm will increase. The result may lose the fidelity. On the contrary, for a small regularization parameter, the optimization algorithm will concentrate on the residual norm $\left\|R(\{p\})-\left\{R^E\right\}\right\|_2^2$ instead in order to reduce the overall misfit effectively. Consequently, the analytical modal parameters are very close to the measured values. The problem may be overfitted, and the solution is not sparse.

In this connection, the regularization parameter should be chosen appropriately by achieving a trade-off between the data fidelity and the sparsity of the solution. The data fidelity measured by the 2-norm of the residue $\left(\left\|R(\{p\})-\left\{R^E\right\}\right\|_2^2\right)$ and the sparsity of the solution is enforced by the 1-norm of the solution ($\|\{p\}\|_1$). Both the the residual norm and solution norm play a crucial role in selecting the optimal regularization parameter. The optimal regularization parameter should keep these two norms small at the same time.

In the Tikhonov regularization, the L-curve criterion utilized a parametric plot of the solution norm versus the residual norm on the log–log scale to find the optimal regularization parameter.[42] The corner of the curve is a good choice of the regularization parameter, which satisfies a small solution norm as well as a small residual norm at the same time. For the l_1 regularization problems, the curves of the residual norm versus the solution norm on the log–log coordinate do not resemble shape L. Inspired by the previous study,[43] these two norms are plotted on the linear scale instead. However, some points on the resulting "L-curve" bunch up and change abruptly because the 1-norm of the solution is not smooth and nondifferentiable. Moreover, because the l_1 regularization does not have a close-form solution, the curvature of the L-curve cannot be expressed explicitly. Therefore, it is difficult to locate the corner of the L-curve to identify an optimal regularization parameter. In this study, the curves of the residual norm and solution norm versus the regularization parameter β are utilized to determine a proper regularization parameter. The process will be demonstrated in the following numerical and experimental examples.

3 | A NUMERICAL EXAMPLE

3.1 | Model description

A six-bay planar truss structure (Figure 1) is first utilized as a numerical preliminary study. The truss is simply supported and consists of 31 bar elements and 14 pin joints, resulting in 25 degrees of freedom in total. The total length and height of the truss is 9.00 m and 1.50 m, respectively. The diagonal bar is 2.12 m long. The cross section of each bar is a square with the dimension of 0.05 m. The mass density and Young's modulus are 2.77×10^3 kg/m^3 and 7.0×10^{10} N/m^2, respectively. The damage is simulated by the reduction of Young's modulus of the element or reduction of the axial stiffness while mass remaining unchanged. In this study, Element 3 is damaged by 50%, that is, $\mathrm{SRF}_3 = -50\%$.

It is assumed that the complete mode shapes at all 25 degrees of freedom are available in the undamaged and damaged states. The first six natural frequencies and mode shapes without noise are first employed for damage identification. In consideration of the measurement noise effect, random noise with the normal distribution is directly added to modal parameters as

$$\widehat{\psi} = (1 + a\mu)\psi \tag{14}$$

where $\widehat{\psi}$ is the noisy modal parameter, ψ is the exact modal parameter, a is the level of noise, and μ follows a normal distribution with a zero mean and variance of 1.0.

Previous studies[31,44] have suggested that natural frequencies may contain 1% noise, and mode shapes may contain 8%–10% noise in practical ambient vibration tests. To examine the effect of noise on the damage detection accuracy and the selection of the regularization parameter, two different levels of noise as listed in Table 1 are introduced into the

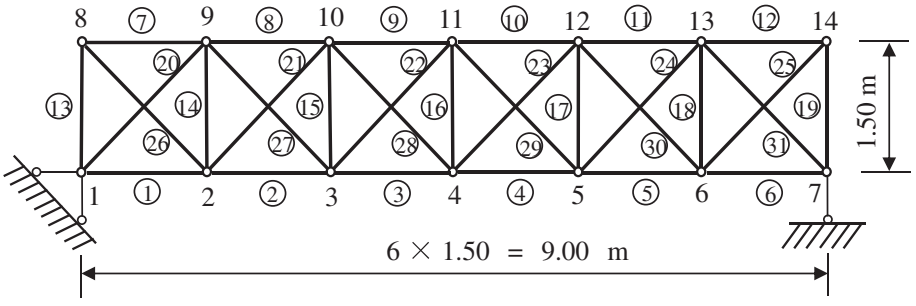

FIGURE 1 Geometric configuration of the truss structure

TABLE 1 Noise levels for the frequency and mode shape

Noise level	Frequency	Mode shape
1	1%	10%
2	2%	20%

frequencies and mode shapes of the damaged structure. The natural frequencies and modal assurance criterion (MAC)[40] of the undamaged and damaged structures are compared in Table 2. It is noted that a few natural frequencies in the damaged states are higher than the undamaged ones due to the random noise.

3.2 | Damage detection with l_1-regularized model updating

3.2.1 | Using noise-free modal data

First, the modal data without any noise are used for damage detection. To select the regularization parameter, the objective function, that is, Equation 11, is solved for different β ranging from 0.005–1.0 with the increment $\Delta\beta = 0.005$. For each β, the associated residual norm and solution norm are then calculated. Because both the frequencies and mode shapes are utilized for model updating, the residual norm consists of the frequency residue and mode shape residue.

The resulting curves of the residual norm and solution norm versus the regularization parameter β are displayed in Figure 2. As described previously, the residual norm increases and solution norm decreases as β increases. When $\beta \geq 0.375$, the solution norm is zero, indicating that no any damage is detected. This is consistent with the previous explanation that there exists a maximal regularization parameter $\beta_{\max}$. Hence, the regularization parameter β should be less than $\beta_{\max}$ in order to obtain a meaningful solution. The residual norm is very close to zero at the beginning and increases gradually with the increase of β. The solution norm drops steadily until reaching the maximal regularization parameter. For the noise-free situation, the regularization parameter should be selected small enough in order to force the updated modal parameters as close to the analytical ones as possible. Therefore, $\beta = 0.005$ is selected as the optimal regularization parameter.

Figure 3 shows the damage identification results for different β. When $\beta = 0$, the damaged Element 3 can be identified, but the severity is incorrect. Also, several undamaged elements are falsely detected as damaged. For $\beta = 0.005$, the damage location and severity can be identified accurately and no false identification occurs. For $\beta = 0.10$, the identification result still has good accuracy. When $\beta = 0.33$, the damaged element can be correctly located whereas the damage

TABLE 2 Frequencies and MAC of the truss in the undamaged and damaged states

		Damaged					
				Noise level 1		Noise level 2	
Mode	Undamaged Freq. (Hz)	No noise Freq. (Hz)	MAC	Freq. (Hz)	MAC	Freq. (Hz)	MAC
1	36.92	34.50 (−6.55)	99.79	34.37 (−6.91)	99.79	33.89 (−8.20)	99.78
2	77.11	76.00 (−1.44)	99.80	76.04 (−1.39)	99.80	75.51 (−2.07)	99.80
3	135.59	135.52 (−0.06)	99.98	136.67 (+0.80)	99.98	133.39 (−1.63)	99.98
4	226.36	217.90 (−3.74)	98.58	221.95 (−1.95)	98.56	216.31 (−4.44)	98.56
5	253.52	252.95 (−0.22)	99.42	250.23 (−1.30)	99.39	253.55 (+0.01)	99.38
6	364.15	361.33 (−0.77)	87.06	361.21 (−0.81)	86.95	362.59 (−0.43)	86.93
Average of frequency change (%)		−2.13	—	−1.92	—	−2.79	—

Note. Values in parentheses are the frequency change ratios (%) between the damaged and undamaged states. MAC = modal assurance criterion.

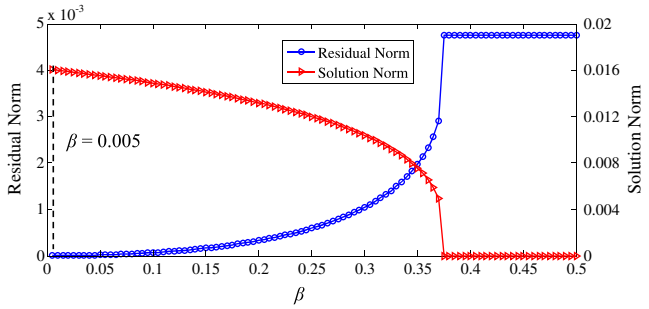

FIGURE 2 Residual norm and solution norm for different β (no noise). SRF = stiffness reduction factor

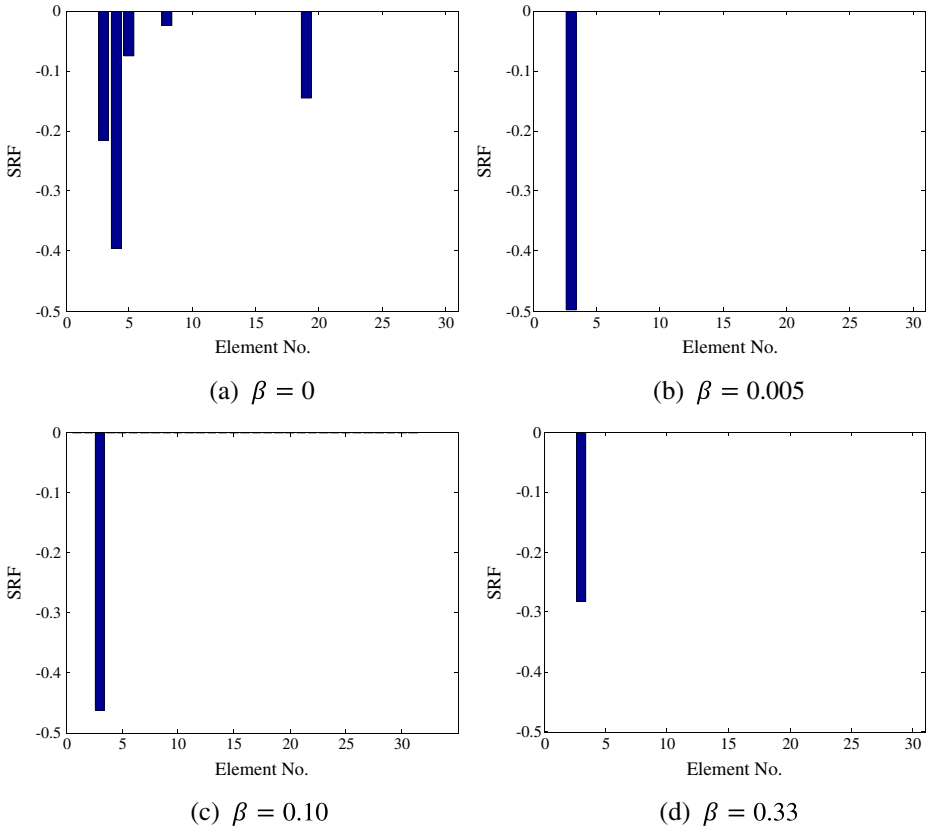

FIGURE 3 Damage identification results (no noise). SRF = stiffness reduction factor

severity differs from the true value. In this example, using the regularization parameter in the range of 0.005 to 0.20 one can obtain satisfactory results.

3.2.2 | Using modal data of noise level 1

When measurement noise is considered, the modal data are generated through Equation 14. For noise level 1 (1% noise for frequencies and 10% for mode shapes), Equation 11 is similarly solved for β ranging from 0.005–1.0. The resulting curves of the residual norm and solution norm versus different β are plotted in Figure 4. With the increase of β, the solution norm decreases rapidly at the beginning, then changes relatively slower from $\beta = 0.03$ to $\beta = 0.20$, and drops quickly until an abrupt step down to zero at $\beta = 0.35$. Therefore, the inflection point $\beta = 0.03$ is selected as the optimal regularization parameter. A close observation shows that $\beta = 0.03$ is also the inflection point of the residual norm curve. At the point, both the residual norm and solution norm are small at the same time.

The damage identification results of SRFs are shown in Figure 5 for different β. When $\beta = 0.01$, the true damage at Element 3 can be identified correctly, whereas the undamaged Elements 10 and 30 are falsely identified as damaged.

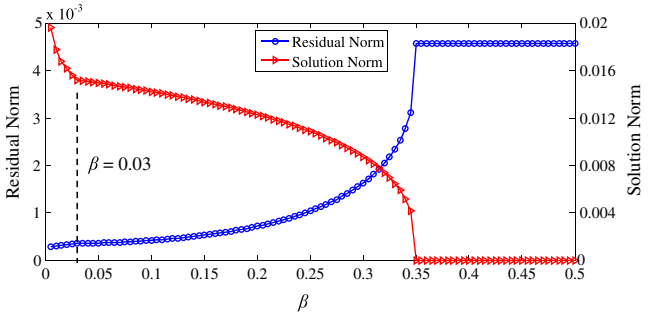

FIGURE 4 Residual norm and solution norm for different β (noise level 1)

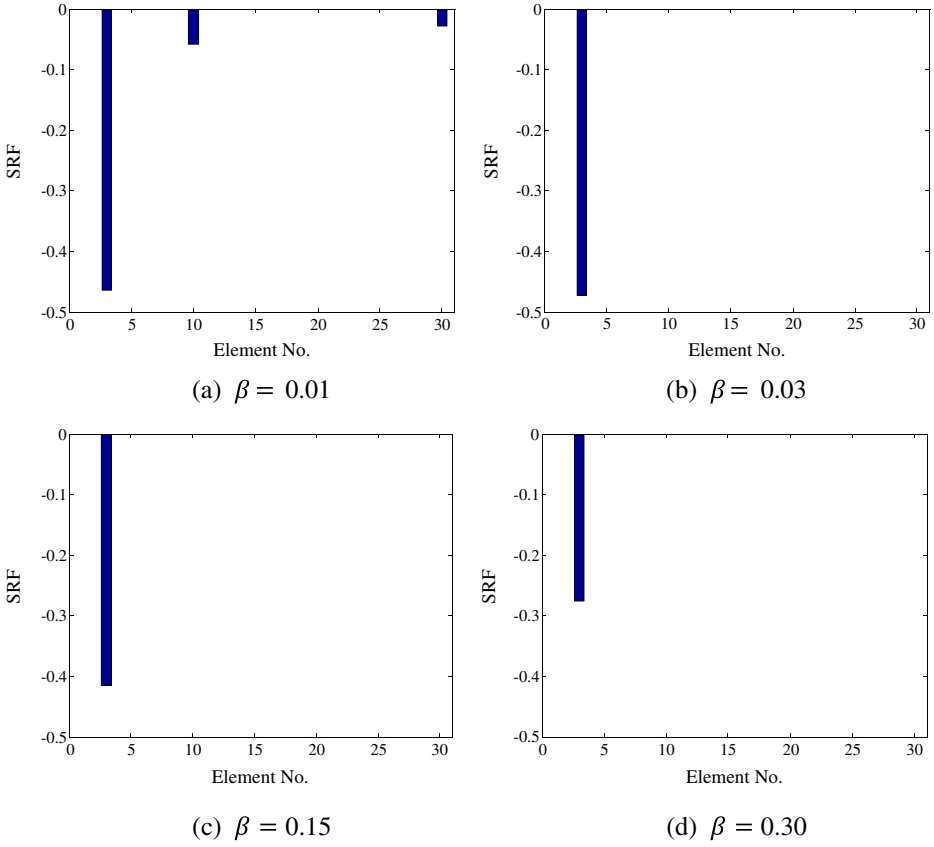

FIGURE 5 Damage identification results (noise level 1). SRF = stiffness reduction factor

For $\beta = 0.03$, the damaged element can be located and quantified accurately with no false identification. For $\beta = 0.15$, the residual norm and solution norm are close to those of $\beta = 0.03$ and the damage detection results are acceptable. When $\beta = 0.30$, although the damaged element is detected, the identified SRF is not accurate.

3.2.3 | Using modal data of noise level 2

In the case of noise level 2 (2% noise for frequencies and 20% for mode shapes), the residual norm and solution norm versus β are illustrated in Figure 6. The shapes of these two curves are similar to those at noise level 1. The inflection point $\beta = 0.055$ is selected as the optimal regularization parameter. The damage identification results are shown in Figure 7 for different β. When $\beta = 0.03$, Element 8 is falsely identified as damaged. For $\beta = 0.055$ and $\beta = 0.12$, the damage location is determined correctly, and the identified SRFs are very close to the true value. Because $\beta = 0.47$ is away from the optimal regularization parameter, the identified damage severity is not correct.

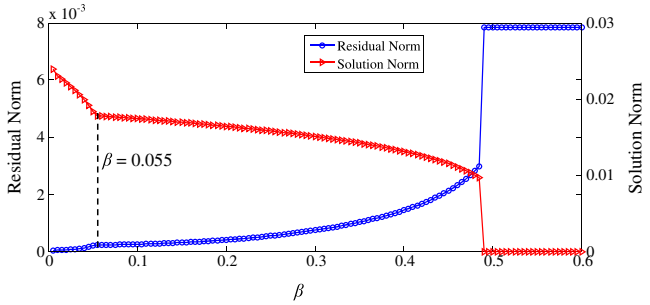

FIGURE 6 Residual norm and solution norm for different β (noise level 2)

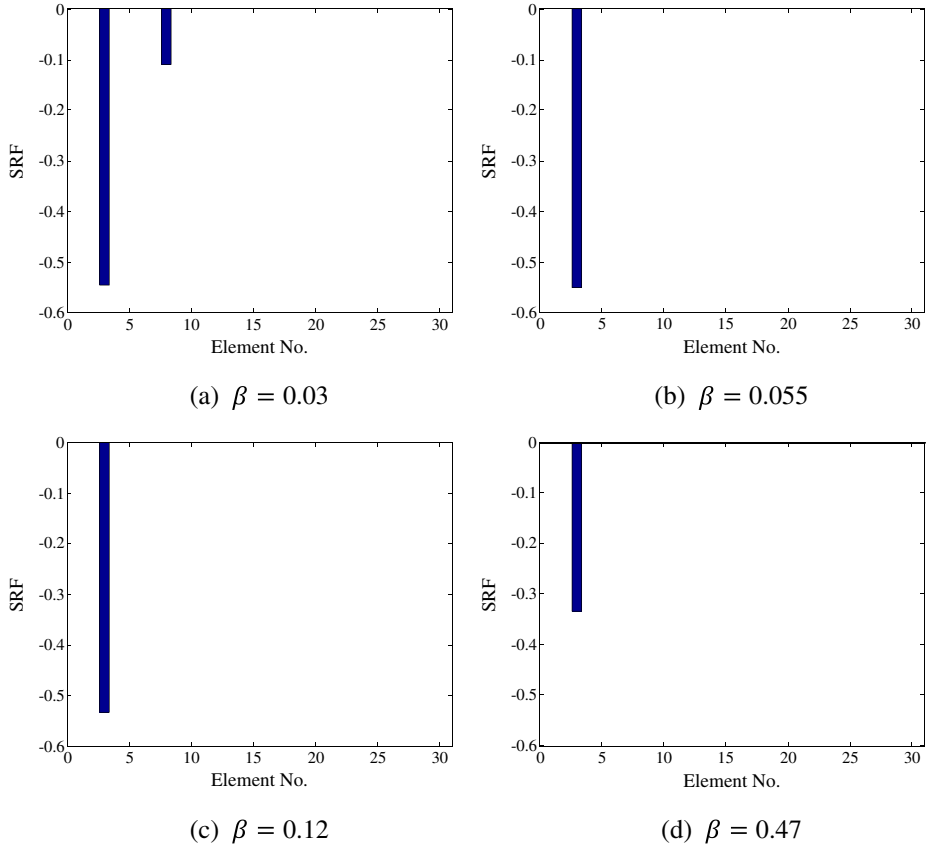

FIGURE 7 Damage identification results (noise level 2). SRF = stiffness reduction factor

The above numerical results show that the developed l_1 regularization-based damage detection technique is effective in locating and quantifying structural damage. In addition, the proposed method has good robustness to noise and works well even under a high noise level. For both noise situations, the damage identification results are accurate when the regularization parameter is selected around the inflection point.

4 | AN EXPERIMENTAL EXAMPLE

4.1 | Descriptions of the experiment

The experimental example is a three-story steel frame as shown in Figure 8. The bottom supports of the columns were welded on a thick plate, which was fixed on the strong floor in order to model the fixed boundary condition of the frame. The overall height of the frame is 1.5 m, and each story is of the same height of 0.5 m. The span of the beam is also 0.5 m. The beams and columns have the same cross section dimension as 75.0×5.0 mm^2. The mass density of the frame is 7.92×10^3 kg/m^3 and the Young's modulus is estimated as 2.0×10^{11} N/m^2.

Accelerometers were used to measure the acceleration signal during the laboratory test. The accelerometer has a magnetic base that enables itself to be firmly mounted on the steel frame. An instrumented hammer with a rubber tip was used to excite the experimental model.

The modal testing was first conducted on the intact frame. The sampling frequency was 2000 Hz, which is adequate for the tested model (the frequency range of interest is about 0–100 Hz). In order to obtain the complete mode shapes of the whole frame, the measurement points were chosen every 100 mm as shown in Figure 9. For the measurement points on the beam and columns, the vertical and horizontal accelerations were measured, respectively. For each beam, only one horizontal vibration was measured at one beam-column joint as the axial deformation of the beam is negligible. There were 39 measurement points in total.

FIGURE 8 Overview of the frame structure

The frame was excited with the hammer, and the direction and location of the excitation point are displayed in Figure 9. After completing the test, a modal analysis was performed with the DIAMOND software.[45] The first eight frequencies and mode shapes in the range of 0–100 Hz were extracted using the rational fraction polynomial method.[46] The natural frequencies and MAC of the experimental model are listed in Table 3.

Four cuts were then sequentially introduced to the frame model (Figure 9). These four cuts were located at beam/column members and their joints that all are critical locations for the frame structure. The enlarged Cut 1 is shown in Figure 10. The saw cuts have the same length $b = 20$ mm and different depths of $d = 22.5$, 22.5, 30, and 30 mm for cuts 1, 2, 3, and 4, respectively. The moment of inertia of the cut sections were then reduced by 60%, 60%, 80%, and 80%. For each damage case, the aforementioned modal testing was repeated and the frequencies and mode shapes of the damaged states were extracted accordingly. The results are listed in Table 4. With the accumulation of damage, the natural frequencies of the structure decrease, so do the MAC values. In addition, the changes in natural frequency are small (maximum average change of 4.13%), whereas the changes in the mode shape are more significant with low MAC values. It can also be seen that the damage in the column members cause larger changes in frequencies and mode shapes than that in the beam members.

4.2 | FE modeling of the frame

As introduced above, most previous studies employ superelements in numerical modeling and model updating. For example, in the study by Hao and Xia,[47] several saw cuts each with 25 mm long were introduced to a portal frame to simulate damage. Euler–Bernoulli beam elements each with 100 mm long were used in the FE model, and the damage was represented by the stiffness reduction of the damaged elements. As the elements are significantly longer than the

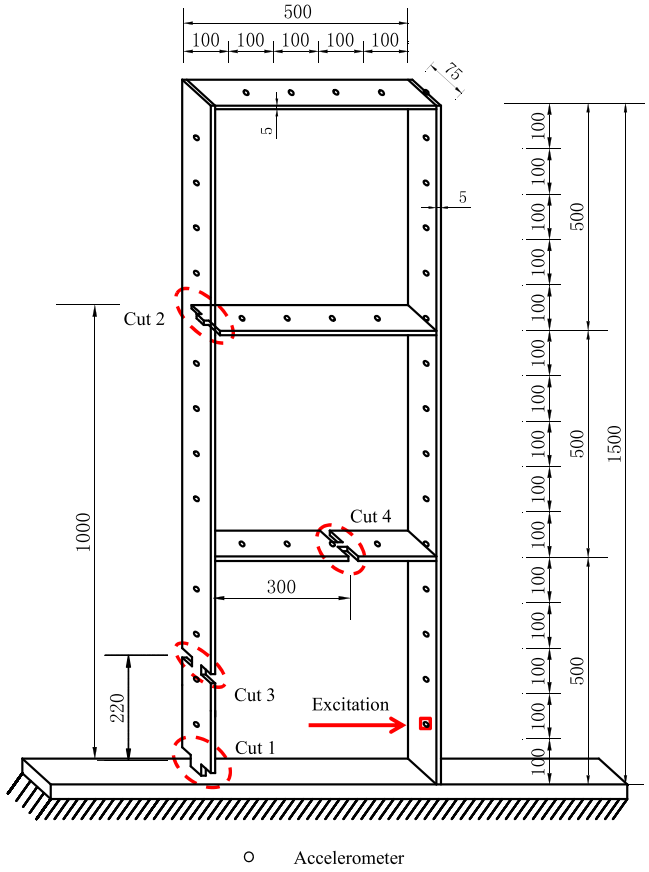

FIGURE 9 Locations of accelerometers and simulated damage (unit: mm)

TABLE 3 Modal data of the experimental model and initial FE model

Mode	Experiment freq. (Hz)	FE model freq. (Hz)	Frequency difference (%)	MAC (%)
1	4.23	3.99	−5.67	98.25
2	14.03	13.19	−5.99	98.54
3	25.45	23.86	−6.25	99.70
4	44.81	42.77	−4.55	92.51
5	58.12	54.67	−5.94	84.31
6	68.36	64.67	−5.40	97.91
7	72.27	67.39	−6.75	93.87
8	91.73	86.50	−5.70	96.94
Average			−5.78	95.25

Note. MAC = modal assurance criterion; FE = finite element.

cuts, a cut of 80% section reduction caused a small stiffness reduction in the corresponding element, and there has been no quantitative relation between the cut size and the element SRF. Consequently, the simulated damage cannot be quantified.

As the l_1 regularization technique is able to maintain the sparsity of the solution using a smaller number of measurements, the structure can be modeled using a relatively large number of elements that enables the local damage to be directly quantified. In this study, the frame is divided into 225 elements, each with 20 mm long. As the length of each cut is identical to the length of one element, the damage severity, quantified by the elemental stiffness reduction, equals to the reduction in the moment of inertia of the cross section. That is, the SRFs of the four cuts are −60%,

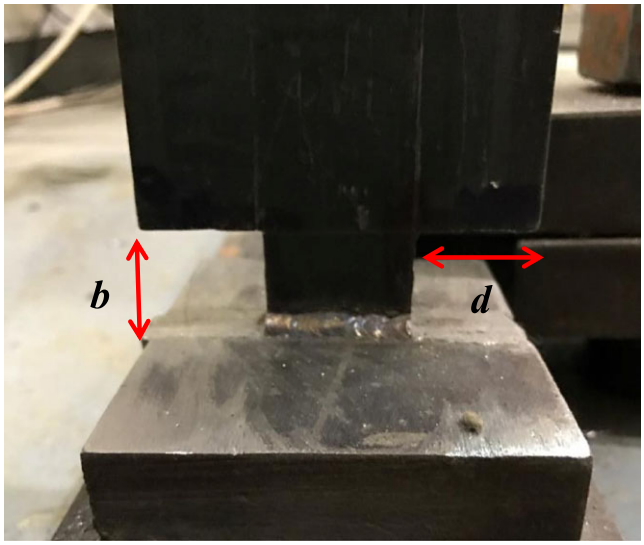

FIGURE 10 Configuration of Cut 1

TABLE 4 Modal data of the undamaged and damaged frame structure

Mode	Undamaged Freq. (Hz)	Damage scenario 1		Damage scenario 2		Damage scenario 3		Damage scenario 4	
		Freq. (Hz)	MAC	Freq. (Hz)	MAC	Freq. (Hz)	MAC	Freq. (Hz)	MAC
1	4.23	4.13 (−2.31)	92.02	4.08 (−3.53)	95.78	4.06 (−3.88)	89.50	4.03 (−4.68)	94.07
2	14.03	13.75 (−1.96)	99.02	13.45 (−4.11)	97.49	13.42 (−4.32)	97.77	13.45 (−4.09)	97.39
3	25.45	25.14 (−1.19)	98.87	25.13 (−1.23)	99.01	25.09 (−1.41)	98.10	25.14 (−1.18)	96.52
4	44.81	44.70 (−0.23)	94.74	44.69 (−0.27)	97.59	44.62 (−0.42)	96.26	44.16 (−1.44)	86.86
5	58.12	57.39 (−1.24)	92.45	57.28 (−1.44)	91.46	56.55 (−2.69)	92.99	55.28 (−4.88)	75.05
6	68.36	67.34 (−1.49)	93.01	66.11 (−3.29)	88.14	65.31 (−4.46)	76.46	65.08 (−4.79)	82.43
7	72.27	72.06 (−0.28)	96.30	71.42 (−1.18)	85.80	70.74 (−2.12)	76.23	69.89 (−3.29)	75.99
8	91.73	89.14 (−2.83)	86.79	88.51 (−3.52)	76.38	84.71 (−7.66)	36.49	83.80 (−8.65)	30.73
Average (%)		−1.44	94.15	−2.32	91.46	−3.37	82.98	−4.13	79.88

Note. MAC = modal assurance criterion.

TABLE 5 SRFs for the four damage scenarios

Case 1	Case 2	Case 3	Case 4
SRF(1) = −60%	SRF(1) = −60%	SRF(1) = −60%	SRF(1) = −60%
	SRF(176) = −60%	SRF(176) = −60%	SRF(176) = −60%
		SRF(12) = −80%	SRF(12) = −80%
			SRF(166) = −80%

Note. SRF = stiffness reduction factor.

−60%, −80%, and −80%. As shown in Figure 9, Cuts 1–4 are located at elements 1, 176, 12, and 166, respectively. The SRFs of the damaged elements for the four damaged scenarios are given in Table 5. There are at most four damaged elements of the structure. Therefore, the actual SRF vector has at most four non-zero items, which is extremely sparse compared to the total 225 elements. Lumped masses are added at the corresponding node to represent the masses of the accelerometers.

In order to reduce the influence of modeling uncertainties of the initial FE model, the measured modal data in the undamaged state were first used to update the initial FE model.[48] No regularization is introduced in this step. The updated model represents a more accurate reference model in the undamaged state as its modal properties agree with the measured ones. The reference FE model will be used for damage detection in the next section.

4.3 | Damage detection with l_1-regularized model updating

To select the regularization parameter, the objective function is solved for different β ranging from 0.01–1.0 with the increment $\Delta\beta = 0.01$. For damage Scenario 1, the residual norm and solution norm versus β are plotted in Figure 11. The solution norm drops sharply at the beginning, whereas the residual norm remains almost unchanged with the increase of β. The inflection point $\beta = 0.06$ is thus selected as the optimal regularization parameter of which the residual norm and solution norm are both small. The regularization parameters for other three damage scenarios are $\beta = 0.12$, 0.11, and 0.09, respectively. The damage identification results for four damage scenarios are shown in Figure 12. For damage Scenario 1, the damage location can be accurately identified with the damage severity slightly larger than the true value (60% reduction). For damage Scenarios 2 and 3, the damaged elements are detected correctly and no false identification occurs, although the SRF of Element 176 has a small error. In damage Scenario 4, three damage locations are correctly detected but Element 166 is not. A number of elements are falsely identified as damaged with small SRF values. As shown in Table 4, the changes in frequencies and mode shapes caused by Cuts 2 and 4 on the beams are smaller than those by Cuts 1 and 3 on the column. Therefore, cuts in the beams are more difficult to be identified than the cuts on the column, due to the existence of measurement noise.

In the previous example, all eight mode shapes at all 39 measurement points were used for damage detection. As l_1 regularization technique is able to deal with underdetermined problems,[13,29,49] we also use three mode shapes to detect damage at Scenario 2. In the case, there are 120 measurement data and 225 unknown SRF values to be identified. Using the proposed l_1 regularization technique, the damage identification results are shown in Figure 13. The two damaged elements are still identified with good accuracy and no false identification occurs. Nevertheless, the number of sensors, number of modes, and sensor locations may have a significant effect on the damage detection.[50] These merit further study in future.

The l_2 regularization technique is also employed here to identify damage for comparison purpose. The following objective function corresponding to Equation 11 is minimized for damage identification

$$\widehat{p} = \arg\min_{\widehat{p}} \left(\frac{1}{m} \sum_{i=1}^{m} \left[\frac{\lambda_i^A(\{p\}) - \lambda_i^E}{\lambda_i^E} \right]^2 + \frac{1}{m \times np} \sum_{i=1}^{m} \sum_{j=1}^{np} \left[\phi_{ji}^A(\{p\}) - \phi_{ji}^E \right]^2 + \frac{\beta}{n} \|\{p\}\|_2^2 \right) \tag{15}$$

The only difference between Equations 15 and 11 is that the 2-norm is used as the solution norm in Equation 15. The regularization parameter β is determined by the L-curve criterion used for the Tikhonov regularization,[47] which is calculated as 0.0301, 0.0292, 0.0278, and 0.0305 for the present four damage scenarios. The damage identification results are displayed in Figure 14. In all cases, the identification results are not sparse, and a considerable number of undamaged elements are falsely identified as damaged. The damaged Element 1 cannot be detected for damage Scenarios 2 and 166

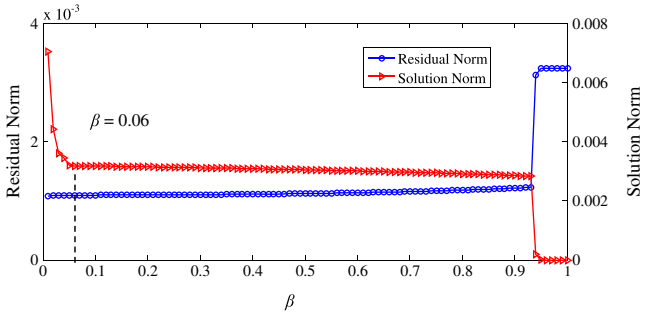

FIGURE 11 Residual norm and solution norm for different β in damage Scenario 1. SRF = stiffness reduction factor

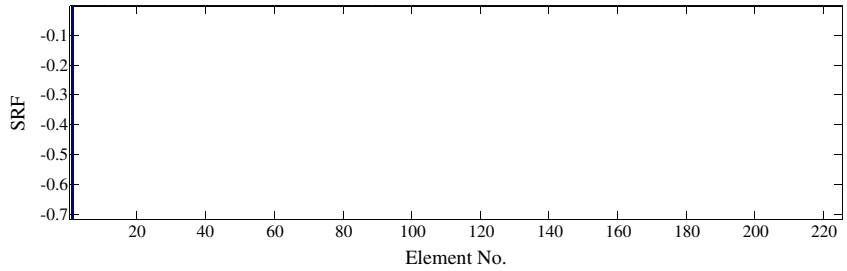

(a) Damage scenario 1 (Damaged element No.1)

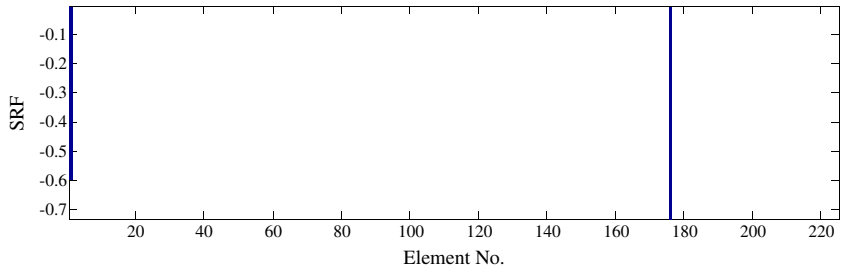

(b) Damage scenario 2 (Damaged element Nos.1 and 176)

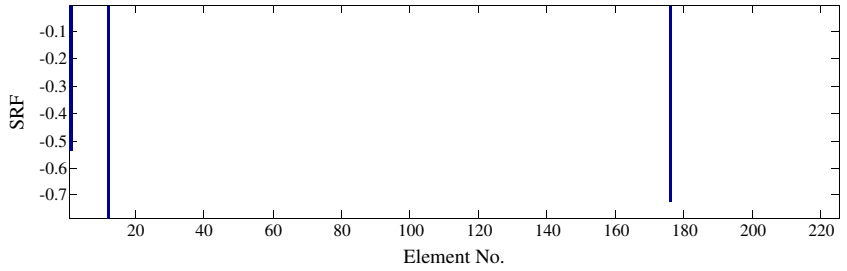

(c) Damage scenario 3 (Damaged element Nos.1, 12 and 176)

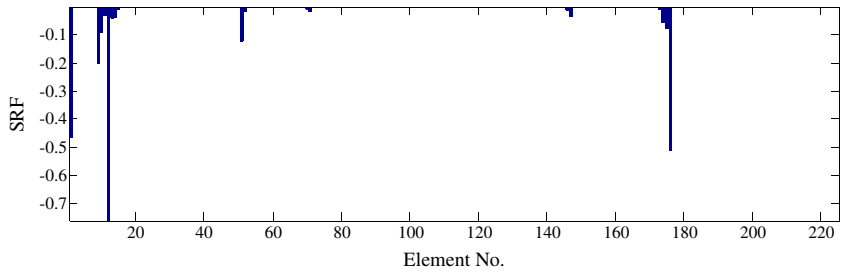

(d) Damage scenario 4 (Damaged element Nos.1, 12, 166 and 176)

FIGURE 12 Damage identification results for four damage scenarios with the l_1 regularization technique

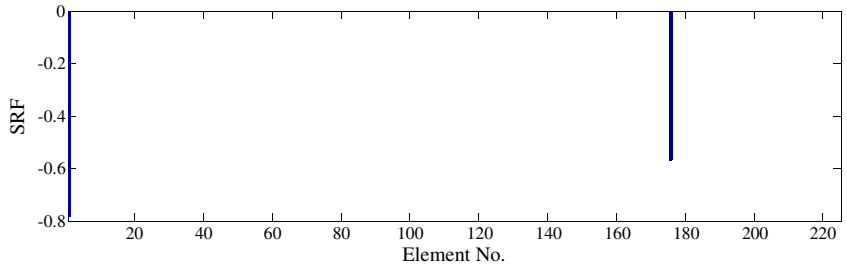

FIGURE 13 Damage identification results for damage Scenario 2 using three frequencies and mode shapes.
SRF = stiffness reduction factor

cannot be identified in all cases. Although the damaged Elements 12 and 176 are detected roughly, the damage severities differ much from the true values (60% and 80%, respectively). The above comparison demonstrates that the l_1 regularization-based damage detection technique is able to identify sparse damaged elements, whereas the l_2 regularization cannot.

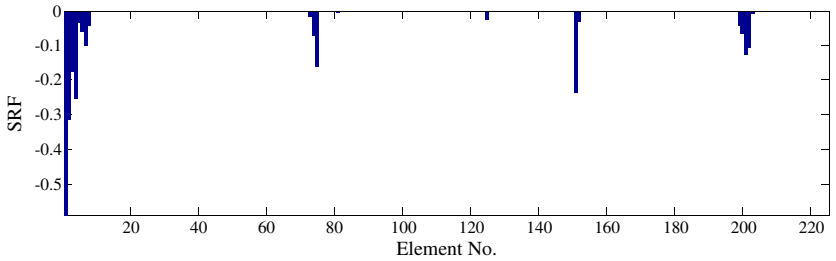

(a) Damage scenario 1 (Damaged element No.1)

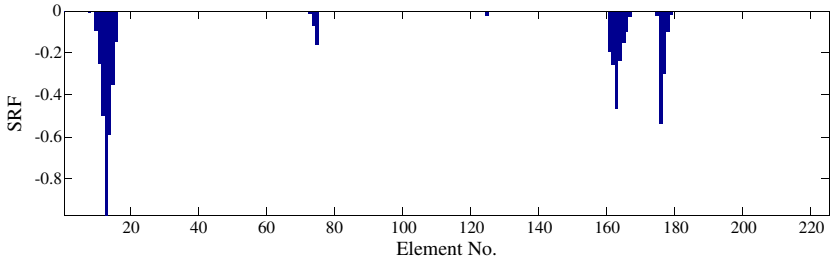

(b) Damage scenario 2 (Damaged element Nos.1 and 176)

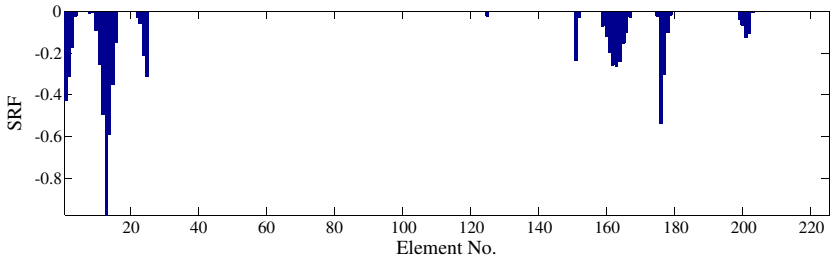

(c) Damage scenario 3 (Damaged element Nos.1, 12 and 176)

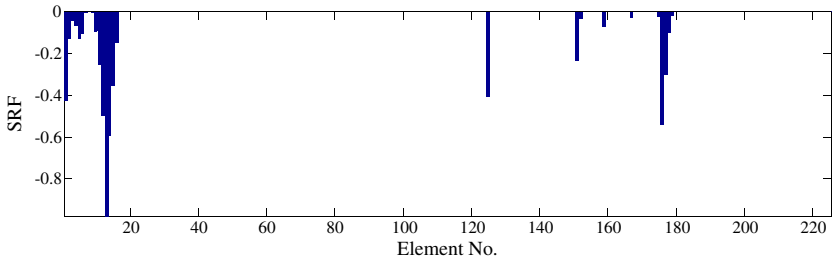

(d) Damage scenario 4 (Damaged element Nos.1, 12, 166 and 176)

FIGURE 14 Damage identification results for four damage scenarios with the l_2 regularization technique. SRF = stiffness reduction factor

5 | CONCLUSIONS AND DISCUSSIONS

A sparse damage detection technique using the natural frequencies and mode shapes is developed. Through exploiting the sparse property of the structural damage, the l_1 regularization technique is employed to identify the sparse damage among a large number of potential elements. The proposed method enables the local damage being directly quantified through using fine elements in the FE modeling. The advantages of using frequency changes and mode shape changes are that frequencies can be measured conveniently and accurately, and mode shapes could provide spatial information of structures and are sensitive to local damage. In addition, a method for selection of the regularization parameter is proposed by examining the residual norm and solution norm curves. A numerical and an experimental examples verify that the proposed sparse damage detection method can successfully identify single and multiple damage, even there are a large number of unknowns. The proposed method is robust to noise even under the severe noise situation.

The examples also demonstrate that the l_1 regularization technique is able to maintain the sparsity of the solution when the number of measurement data is much less than the number of elements. Therefore, the structure of interest can be modeled with a relatively large number of elements, such that a local damage can be directly modeled and the damage severity can be quantified by the elemental stiffness reduction. Although the proposed method cannot identify

all damage accurately, it is advantageous over the traditional l_2 regularization technique. Further studies may give to the number of sensors, number of modes, and sensor locations. Applications to large-scale practical structures will also be carried out.

ACKNOWLEDGEMENTS

This research was supported by the PolyU Research Grant (Projects 1-ZVDN and G-YBHL) and the National Natural Science Foundation of China (Project 51678364).

ORCID

Yong Xia http://orcid.org/0000-0001-5319-5858

REFERENCES

[1] Doebling SW, Farrar CR, Prime MB, Shevitz DW. Damage identification and health monitoring of structural and mechanical systems from changes in their vibration characteristics: A literature review, *Los Alamos National Laboratory Report*, **1996**.

[2] Sohn H, Farrar CR, Hemez FM, Shunk DD, Stinemates DW, Nadler BR, Czarnecki JJ. A review of structural health monitoring literature: 1996–2001, *Los Alamos National Laboratory Report*, **2003**.

[3] O. S. Salawu, *Eng. Struct.* **1997**, *19*(9), 718.

[4] J. T. Kim, N. Stubbs, *J. Sound Vib.* **2003**, *259*(1), 145.

[5] Z. Shi, S. Law, L. Zhang, *J. Eng. Mech.* **2000**, *126*(6), 656.

[6] Y. Xia, H. Hao, A. J. Deeks, X. Zhu, *J. Bridg. Eng.* **2008**, *13*(1), 43.

[7] A. Pandey, M. Biswas, M. Samman, *J. Sound Vib.* **1991**, *145*(2), 321.

[8] A. Pandey, M. Biswas, *J. Sound Vib.* **1994**, *169*(1), 3.

[9] Y. Xia, H. Hao, A. J. Deeks, *Eng. Struct.* **2007**, *29*(7), 1475.

[10] H. Ahmadian, J. Mottershead, M. Friswell, *Mech. Syst. Signal Process.* **1998**, *12*(1), 47.

[11] B. Weber, P. Paultre, J. Proulx, *Mech. Syst. Signal Process.* **2009**, *23*(6), 1965.

[12] X. Li, S. Law, *Mech. Syst. Signal Process.* **2010**, *24*(6), 1646.

[13] E. J. Candès, Compressive sampling, *Proceedings of the International Congress of Mathematicians*, Madrid, Spain, **2006**, 1433–1452.

[14] D. L. Donoho, *IEEE Trans. Inf. Theory* **2006**, *52*(4), 1289.

[15] R. G. Baraniuk, *Science* **2011**, *331*(6018), 717.

[16] Y. Bao, J. L. Beck, H. Li, *Struct. Health Monit.* **2011**, *10*(3), 235.

[17] Y. Bao, H. Li, X. Sun, Y. Yu, J. Ou, *Struct. Health Monit.* **2013**, *12*, 78.

[18] Y. Bao, Y. Yu, H. Li, X. Mao, W. Jiao, Z. Zou, J. Ou, *Struct. Control Health Monit.* **2015**, *22*(3), 433.

[19] Y. Bao, H. Li, Z. Chen, F. Zhang, A. Guo, *Struct. Control Health Monit.* **2016**, *23*(1), 144.

[20] Z. Zou, Y. Bao, H. Li, B. F. Spencer, J. Ou, *IEEE Sens. J.* **2015**, *15*(2), 797.

[21] Y. Wang, H. Hao, An introduction to compressive sensing and its potential applications in structural engineering, *The 11th International Symposium on Structural Engineering*, Guangzhou, China, 18–20 December **2010**, 1089–1094.

[22] Y. Yang, S. Nagarajaiah, *Struct. Control Health Monit.* **2014**, *21*(6), 962.

[23] Y. Yang, S. Nagarajaiah, *J. Sound Vib.* **2013**, *332*(19), 4741.

[24] Y. Yang, S. Nagarajaiah, *Mech. Syst. Signal Process.* **2015**, *56*, 15, https://doi.org/10.1016/j.ymssp.2014.10.015.

[25] Y. Huang, J. L. Beck, H. Li, S. Wu, Robust diagnostics for Bayesian compressive sensing with applications to structural health monitoring, In: *Proceedings of the SPIE 7982, smart sensor phenomena, technology, networks, and systems*, San Diego, CA, USA, **2011**.

[26] Y. Bao, H. Li, J. Ou, *J Civil Struct. Health Monit.* **2014**, *2*(4), 77.

[27] Y. Yang, S. Nagarajaiah, *Mech. Syst. Signal Process.* **2014**, *45*(1), 1.

[28] E. M. Hernandez, *Mech. Syst. Signal Process.* **2014**, *46*(1), 59.

[29] X. Q. Zhou, Y. Xia, S. Weng, *Struct. Health Monit.* **2015**, *14*(6), 571.

[30] C. Zhang, Y. Xu, *Struct. Control Health Monit.* **2016**, *23*(3), 560.

[31] J. Mottershead, M. Friswell, *J. Sound Vib.* **1993**, *167*(2), 347.

[32] P. G. Bakir, E. Reynders, G. De Roeck, *J. Sound Vib.* **2007**, *305*(1), 211.

[33] P. Cawley, R. D. Adams, *J. Strain Anal. Eng. Des.* **1979**, *14*(2), 49.

[34] R. B. Nelson, *AIAA J.* **1976**, *14*(9), 1201.

[35] S. Weng, Y. Xia, Y. L. Xu, H. P. Zhu, *J. Sound Vib.* **2011**, *330*(14), 3368.

[36] Y. Xia, S. Weng, Y. L. Xu, H. P. Zhu, *Struct. Eng. Mech.* **2010**, *36*(1), 37.

[37] F. Bauer, M. A. Lukas, *Math. Comput. Simul.* **2011**, *81*(9), 1795.

[38] R. Sampaio, N. Maia, J. Silva, *J. Sound Vib.* **1999**, *226*(5), 1029.

[39] S. Boyd, L. Vandenberghe, *Convex optimization*, Cambridge University Press, New York, NY **2004**.

[40] R. J. Allemang, *Sound Vib.* **2003**, *37*(8), 14.

[41] K. Koh, S. J. Kim, S. Boyd, *J. Mach. Learn. Res.* **2007**, *8*(Jul), 1519.

[42] P. C. Hansen, *SIAM Rev.* **1992**, *34*(4), 561.

[43] H. Yao, P. Gerstoft, P. M. Shearer, C. Mecklenbräuker, *Geophys. Res. Lett.* **2011**, *38*, L20310.

[44] M. Friswell, J. E. Penny, The practical limits of damage detection and location using vibration data, *Proceedings of the 11th VPI and SU Symposium on Structural Dynamics and Control*, Blacksburg, Virginia, **1997**, 31–40.

[45] S. W. Doebling, C. R. Farrar, P. J. Cornwell, DIAMOND: A graphical interface toolbox for comparative modal analysis and damage identification, *Proceedings of the 6th International Conference on Recent Advances in Structural Dynamics*, Southampton, UK, **1997**, 399–412.

[46] D. Formenti, M. Richardson, Parameter estimation from frequency response measurements using rational fraction polynomials (twenty years of progress), *Proceedings of International Modal Analysis Conference*, Orlando, Florida, **2002**, 167–181.

[47] H. Hao, Y. Xia, *J. Comput. Civ. Eng. ASCE* **2002**, *16*(3), 222.

[48] Y. Xia, H. Hao, *J. Sound Vib.* **2003**, *263*(4), 853.

[49] Theodoridis S, Kopsinis Y, Slavakis K. Sparsity-aware learning and compressed sensing: An overview. Acad Press Libr Singnal Process: 1, 1271–1377, **2012**.

[50] S. Zhou, Y. Bao, H. Li, Structural damage identification based on substructure sensitivity and l_1 sparse regularization, Civil Structural Health Monitoring Workshop (CSHM-4), **2013**.

How to cite this article: Hou R, Xia Y, Zhou X. Structural damage detection based on l_1 regularization using natural frequencies and mode shapes. *Struct Control Health Monit*. 2018;25:e2107. https://doi.org/10.1002/stc.2107